BISTABLE COLLAPSIBLE TUBULAR MAST BOOMS

Juan M. Fernandez[(1)], Andrew J. Lee[(2)]

[(1)]NASA Langley Research Center
Structural Dynamics Branch, NASA LaRC, 4 West Taylor Street, Mail Stop 230, Hampton, VA 23681, USA
juan.m.fernandez@nasa.gov

[(2)]University of Michigan
Department of Aerospace Engineering, University of Michigan, 1320 Beal Ave., Ann Arbor, MI 48109 USA
ajle@umich.edu

ABSTRACT

A promising candidate for deployable composite structures is the two-shelled Collapsible Tubular Mast (CTM) boom, which is to be employed on future solar sail and interplanetary small satellite platforms by the National Aeronautics and Space Administration (NASA). This is due to its two omega-shaped shells forming a closed-section which yields large stiffnesses that allowed for high dimensional stability. An inextensional analytical model describing the bending deformation mechanics of CTM booms was used to determine how design variables induce bistability, or the existence of two strain energy wells. Bistable booms were favorable due to low strain energy requirements for the coiled state and had more controllable deployment when compared to monostable booms. The effects of varying lamina material, laminate layup, and shell arc geometries between different inner and outer shell segments on the second strain energy well and stiffness properties were determined for cross-sections formed by circular segments. The full design space for two-shelled composite CTM booms was explored to evaluate the validity of the simple analytical model developed. Optimal CTM boom designs were manufactured and experimentally characterized for comparisons against model results. The model under-predicted the second stable coiled diameter of the complete two-shelled booms by 27-33% and as low as 3-8% for the individual shells wrapped alone.

1. INTRODUCTION

Given their superior structural performance capabilities amongst other thin-shell deployable boom designs, the closed-section tubular masts with joined omega-shaped walls have been the rollable boom design most investigated since its inception in the United States in the 1960s [1]. The first notable use in Space for this boom type was to collect soil samples on Mars during the Viking 1 and 2 missions in 1976 [2]. These Collapsible Tubular Masts (CTM) were constructed from thin metal sheet. Aside from some early investigations in the late 1970s to fabricate these booms using carbon fiber reinforced plastic (CFRP) [3], the first CFRP CTM booms were developed by Sener in Spain in the mid-1980s under the European Space Agency (ESA) umbrella [4]. ESA also spent significant funds developing a continuous manufacturing method for these CTM booms to create very large structures [5]. In the late 1990s, DLR rekindled the boom concept for solar sail applications using more modern composite materials and analysis software packages. Since then, both scaled up [6] and scaled down [7] versions of the early booms have been developed by DLR, although none of them have yet been able to prove their worth in Space.

NASA is currently investing [8] in developing various CTM boom designs fabricated from state of the art thin-ply composite materials that allow multi-layer laminates to be employed for more design control and structural capability. These booms are a promising cross-cutting technology candidate for a wide range of deployable space structures for small satellite applications given their compact nature [9]. A near-term target application of interest is to use them to deploy, tension and support solar sails for deep space science and exploration missions on CubeSat platforms [9]. CTM booms in the 14-16.5 m length range are being developed to enable larger mission-capable solar sailcrafts [10]. Smaller booms up to 7 m in length are also being designed for precursor exploratory or risk-reduction missions [11]. A CTM boom sized under NASA's Near Earth Asteroid (NEA) Scout solar sail mission requirements [9] is shown in Fig. 1 (a).
A recent effort showed how to induce bistability, or the existence of two strain energy wells in the deployed and coiled boom states, into two-shelled rollable boom structures [12]. Bistable booms were favored due to low strain energy requirements for the coiled state, and had a more controllable self-deployment compared to monostable booms that enabled more reliable, compact, and lighter system designs. The current research and development effort aimed to produce bistable CTM booms (Bi-CTM) as the ultimate candidate for these types of coilable structures. A simple analytical model that described the mechanics of deformation of the booms was developed in an effort to use parametric analyses to find

and study efficiently structurally optimized CTM designs that also resulted in bistable configurations. Several optimized Bi-CTM boom designs were fabricated and used to evaluate the validity of the analytical modeling tool.

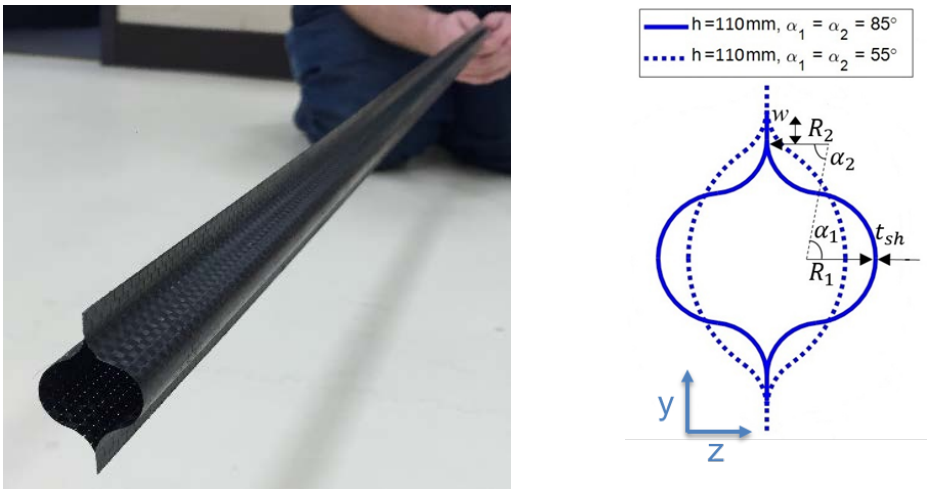

(a) (b)

Fig. 1. (a) Mini-CTM boom initially designed for NEA Scout; (b) Cross-section shapes of two CTM booms with a flattened height of *h = 110 mm* and subtended angles of *α = 85°* (solid line) and *α = 55°* (dashed line). The cross-section is created by joining at the web area, w, two omega-shaped shells of thickness t_{sh} formed by three tangent circular arc segments: a central one defined by radius R_1 and subtended angle α_1 and two edge ones defined by radius R_2 and subtended angle α_2.

2. STABILITY ANALYTICAL MODEL

The method for predicting the stable coiled diameter and strain energy states of the Bi-CTM boom was extended from a simple strain energy analytical model of cylindrical shells [13]. It assumed that the shell was under plane stress and its initial configuration was stress free. In addition, the shell's mid-surface bent without stretching, which means that all deformations were uniform, inextensional, and the Gaussian curvature remained unchanged. This also implies that during the deformation process, every possible configuration of the shell could be fitted to the surface of an underlying cylinder, as shown in Fig. 2 (a). Thus, these configurations could be defined by only two parameters: the curvature C of the underlying cylinder, and the orientation angle (θ) of the shell relative to the cylinder's axial axis.

The Bi-CTM's cross sectional parameters were established in order to determine the strain energy terms of each shell segment. For both the inner and outer boom shells, where inner/outer denoted the wall closest/farthest from the coiling spool, let segment 1 be associated with the initial radius of curvature R_1 and subtended angle α_1 and segment 2 with R_2 and α_2, as shown in Fig. 1 (b). To maintain tangent continuity and prevent kinks between segments 1 and 2, α_1 must equal α_2, which means only a single subtended angle and either R_1 or R_2 could be specified. Let h be the flattened height of each shell and w be the width of the web, which is the flat bonded region between both shells. Using the circular arc length equations and the relationship between h, w, and the arc lengths of segments 1 and 2 as given by L_1 and L_2 shown below, the unspecified radius was found. Tangent continuity between shell segments could not be guaranteed if both radii were specified instead.

$$h = 2\,(w + L_1 + L_2) \tag{1}$$

$$L_{1,2} = R_{1,2}\alpha_{1,2} \tag{2}$$

To allow varying cross-sectional geometries, layups, and materials for the Bi-CTM, the radii, lengths, subtended angles, and bending stiffnesses of each shell segment were differentiated between the outer and inner shells and denoted by the $_O$ and $_I$ subscripts. Only the flattened height and web widths were identical between the two shells. Assuming the initial manufactured radius of each segment did not change after bonding, the non-dimensional changes in curvature of segments 1 and 2 for both the outer and inner shells in the $x - y$ coordinate system presented in Fig. 2 (a) and using the Mohr's circle of curvature as shown in Fig. 2 (b) are specified as $\hat{\boldsymbol{k}}_{1_{O,I}}$ and $\hat{\boldsymbol{k}}_{2_{O,I}}$ in (3) and (4). The variation or delta for each segment was between the initially extended configuration at $\theta = 0$ and the final coiled configuration at $0 < \theta < \pi$.

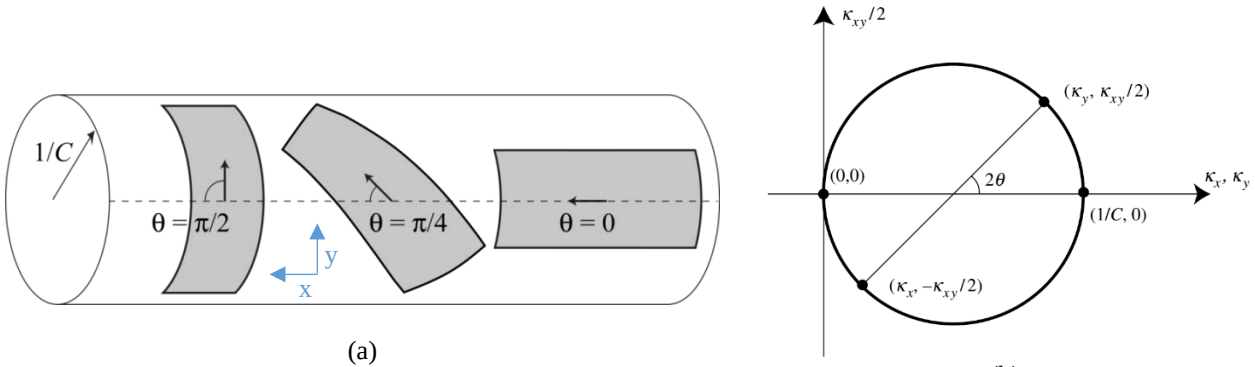

Fig. 2. (a) Coordinate system defining shell configurations on an underlying cylinder of curvature *C*; (b) Mohr's circle of curvature [13]. The vertical axis was $\kappa_{xy}/2$ rather than κ_{xy}, as lamination theory definition of twist was being used.

$$\hat{\boldsymbol{k}}_{1_{O,I}} = R_{1_O}\Delta\begin{bmatrix}\kappa_x\\ \kappa_y\\ \kappa_{xy}\end{bmatrix} = \frac{\hat{C}R_{1_{O,I}}}{2R_{1_O}}\begin{bmatrix}\pm(1-\cos 2\theta)\\ \cos 2\theta + 1 - \frac{2}{\hat{C}}\\ 2\sin 2\theta\end{bmatrix} \tag{3}$$

$$\hat{\boldsymbol{k}}_{2_{O,I}} = R_{1_O}\Delta\begin{bmatrix}\kappa_x\\ \kappa_y\\ \kappa_{xy}\end{bmatrix} = \frac{\hat{C}R_{2_{O,I}}}{2R_{1_O}}\begin{bmatrix}\mp(1-\cos 2\theta)\\ \cos 2\theta + 1 - \frac{2}{\hat{C}}\\ 2\sin 2\theta\end{bmatrix} \tag{4}$$

Every shell segment was normalized by R_{1_O} with $\hat{C} = CR_{1_O}$, where all non-dimensional variables were written with a ˆ symbol. This assumes that the changes in curvature of each segment was linearly proportional to that of the outer shell segment 1 based on the ratio of radii between the segments. Segments bending in the equal-sense way included the outer shell segment 1 and inner shell segment 2, and their changes in κ_x were positive. Segments bending in the opposite-sense way were the outer shell segment 2 and inner shell segment 1, and they retained negative changes in κ_x. Since the two web sections remained flat in the *y*-direction, their non-dimensional changes in curvature were given in (5):

$$\hat{\boldsymbol{k}}_w = \frac{\hat{C}}{2}\begin{bmatrix}1-\cos 2\theta\\ 0\\ 2\sin 2\theta\end{bmatrix} \tag{5}$$

The circular Bi-CTM's bending strain energy per unit length was the sum of the strain energy terms of every shell segment and web sections as given by (7). As shown in (6), it was non-dimensionalized in terms of the flattened height of each shell h, and the bending stiffness $D_{1_{O_{11}}}$ in the x-direction and initial radius of curvature R_{1_O} of the outer shell segment 1. The subscript $_A$ denotes the adhesive layer in the web sections.

$$\hat{U} = \frac{UR_{1_O}{}^2}{hD_{1_{O_{11}}}}, \quad \hat{\boldsymbol{D}}_{O,I,A} = \frac{\boldsymbol{D}_{O,I,A}}{D_{1_{O_{11}}}}, \quad \hat{C} = CR_{1_O} \tag{6}$$

$$\hat{U} = \frac{1}{h}\left[L_{1_O}\hat{\boldsymbol{k}}_{1_O}^T\hat{\boldsymbol{D}}_{1_O}\hat{\boldsymbol{k}}_{1_O} + L_{2_O}\hat{\boldsymbol{k}}_{2_O}^T\hat{\boldsymbol{D}}_{2_O}\hat{\boldsymbol{k}}_{2_O} + L_{1_I}\hat{\boldsymbol{k}}_{1_I}^T\hat{\boldsymbol{D}}_{1_I}\hat{\boldsymbol{k}}_{1_I} + L_{2_I}\hat{\boldsymbol{k}}_{2_I}^T\hat{\boldsymbol{D}}_{2_I}\hat{\boldsymbol{k}}_{2_I} + w\hat{\boldsymbol{k}}_w^T\left(\hat{\boldsymbol{D}}_{w_O} + \hat{\boldsymbol{D}}_{w_I} + \hat{\boldsymbol{D}}_A\right)\hat{\boldsymbol{k}}_w\right] \tag{7}$$

It should be noted that the 3-by-3 ***D*** matrix of each shell segment was the reduced bending stiffness matrix from Classical Lamination Theory (CLT) defined in (8), allowing coupling between bending and stretching in case any of the studied shells had a non-zero ***B*** matrix. If ***B* = 0, *D**** reduces to ***D*** and the in-plane strains are zero.

$$\boldsymbol{D}^* = \boldsymbol{D} - \boldsymbol{B}^T\boldsymbol{A}^{-1}\boldsymbol{B} \tag{8}$$

With the total strain energy per unit length assembled, finding the energy minimizing equilibria involved taking the variation of $\hat{U}$ with respect to the two configuration defining parameters, $\hat{C}$ and θ, as shown in (9):

$$\delta\hat{U} = \frac{\partial\hat{U}}{\partial\theta}\delta\theta + \frac{\partial\hat{U}}{\partial\hat{C}}\delta\hat{C} = 0\,. \tag{9}$$

To satisfy (9), it was necessary to impose the following conditions, whose solutions defined the configurations under equilibrium:

$$\frac{\partial \hat{U}}{\partial \theta} = 0, \quad \frac{\partial \hat{U}}{\partial \hat{C}} = 0 \, . \tag{10}$$

The stability of the solutions was determined by considering the non-dimensional stiffness matrix of the Bi-CTM boom in (11). The configuration was stable if $\widehat{K}$ was positive definite.

$$\widehat{K} = \begin{bmatrix} \frac{\partial^2 \hat{U}}{\partial \theta^2} & \frac{\partial^2 \hat{U}}{\partial \theta \partial \hat{C}} \\ \frac{\partial^2 \hat{U}}{\partial \theta \partial \hat{C}} & \frac{\partial^2 \hat{U}}{\partial \hat{C}^2} \end{bmatrix} \tag{11}$$

3. BOOM DESIGN METRICS

3.1. Bistability Criterion

To directly evaluate the bistability of CTM booms without the need for minimizing the strain energy of every design configuration during parametric studies, a bistability criterion was derived. Assuming there is no coupling between bending and twisting ($D_{16} = D_{26} = 0$) in either the outer or inner shell, the solution to (10) at $\theta = \frac{\pi}{2}$ and the corresponding $\hat{C}$ was the coiled configuration of the second equilibrium position. The initial extended configuration of the first equilibrium position was always stable at $\theta = 0$ and $\hat{C} = 1$. The bistability criterion was derived from checking if $\widehat{K}$ in (11) was positive definite for the second equilibrium position, which was done by evaluating the conditions below.

$$\frac{\partial^2 \hat{U}}{\partial \theta^2} > 0, \quad \frac{\partial^2 \hat{U}}{\partial \hat{C}^2} > 0, \quad \left(\frac{\partial^2 \hat{U}}{\partial \hat{C}^2}\right)\left(\frac{\partial^2 \hat{U}}{\partial \theta^2}\right) > \left(\frac{\partial^2 \hat{U}}{\partial \theta \partial \hat{C}}\right)^2 . \tag{12}$$

Before the criterion was evaluated, the existence of an equilibrium solution at $\theta = \frac{\pi}{2}$ was verified if $\hat{C} > 0$. In (12), $\frac{\partial^2 \hat{U}}{\partial \theta \partial \hat{C}}$ was zero and $\frac{\partial^2 \hat{U}}{\partial \hat{C}^2}$ was always positive. Therefore, the second equilibrium position was stable and the boom was bistable if $\frac{\partial^2 \hat{U}}{\partial \theta^2} > 0$ was satisfied in addition to $\hat{C} > 0$. The circular Bi-CTM boom's bistability criterion was given below through $\hat{C}$ at $\theta = \frac{\pi}{2}$, $\frac{\partial^2 \hat{U}}{\partial \hat{C}^2}$, and $\frac{\partial^2 \hat{U}}{\partial \theta^2}$ in terms of the non-dimensionalized parameters. Note that the radius of every segment was normalized by R_{1_O} and this was denoted with a ˆ (e.g. $\hat{R}_{2_O} = R_{2_O}/R_{1_O}$). The non-dimensional curvature of the coiled state and the bistability criterion depended on the arc lengths and radii of every circular segment, web length, as well as the bending stiffnesses of both shells.

$$\hat{C} = \frac{\hat{D}_{1_{O_{12}}} L_{1_O} - \hat{D}_{1_{I_{12}}} L_{1_I} \hat{R}_{1_I}^2 + \hat{D}_{2_{I_{12}}} L_{2_I} \hat{R}_{2_I}^2 - \hat{D}_{2_{O_{12}}} L_{2_O} \hat{R}_{2_O}^2}{\hat{D}_{1_{O_{11}}} L_{1_O} + \hat{D}_{1_{I_{11}}} L_{1_I} \hat{R}_{1_I}^2 + \hat{D}_{2_{I_{11}}} L_{2_I} \hat{R}_{2_I}^2 + \hat{D}_{2_{O_{11}}} L_{2_O} \hat{R}_{2_O}^2 + w\left(\hat{D}_{\mathrm{w}_{I_{11}}} + \hat{D}_{\mathrm{w}_{O_{11}}} + \hat{D}_{A_{11}}\right)} > 0 \tag{13}$$

$$\frac{\partial^2 \hat{U}}{\partial \hat{C}^2} = \frac{2}{h}\left[L_{1_O} + \hat{D}_{1_{I_{11}}} L_{1_I} \hat{R}_{1_I}^2 + \hat{D}_{2_{I_{11}}} L_{2_I} \hat{R}_{2_I}^2 + \hat{D}_{2_{O_{11}}} L_{2_O} \hat{R}_{2_O}^2 + w\left(\hat{D}_{\mathrm{w}_{I_{11}}} + \hat{D}_{\mathrm{w}_{O_{11}}} + \hat{D}_{A_{11}}\right)\right] > 0 \tag{14}$$

$$\frac{\partial^2 \hat{U}}{\partial \theta^2} = -\frac{4\hat{C}}{h}\left[\begin{array}{l} L_{1_O}\left(\hat{D}_{1_{O_{22}}} - \hat{D}_{1_{O_{12}}}\right) + L_{1_I} \hat{R}_{1_I}^2 \left(\hat{D}_{1_{I_{12}}} + \hat{D}_{1_{I_{22}}}\right) + L_{2_I} \hat{R}_{2_I}^2 \left(\hat{D}_{2_{I_{22}}} - \hat{D}_{2_{I_{12}}}\right) + L_{2_O} \hat{R}_{2_O}^2 \left(\hat{D}_{2_{O_{12}}} + \hat{D}_{2_{O_{22}}}\right) \\ +\hat{C}\left(\begin{array}{l} L_{1_O}\left(1 - \hat{D}_{1_{O_{12}}} - 2\hat{D}_{1_{O_{66}}}\right) + L_{1_I} \hat{R}_{1_I}^2 \left(\hat{D}_{1_{I_{11}}} + \hat{D}_{1_{I_{12}}} - 2\hat{D}_{1_{I_{66}}}\right) + L_{2_I} \hat{R}_{2_I}^2 \left(\hat{D}_{2_{I_{11}}} - \hat{D}_{2_{I_{12}}} - 2\hat{D}_{2_{I_{66}}}\right) \\ +L_{2_O} \hat{R}_{2_O}^2 \left(\hat{D}_{2_{O_{11}}} + \hat{D}_{2_{O_{12}}} - 2\hat{D}_{2_{O_{66}}}\right) + w\left(\hat{D}_{\mathrm{w}_{I_{11}}} + \hat{D}_{\mathrm{w}_{O_{11}}} + \hat{D}_{A_{11}} - 2\hat{D}_{\mathrm{w}_{I_{66}}} - 2\hat{D}_{\mathrm{w}_{O_{66}}} - 2\hat{D}_{A_{66}}\right) \end{array}\right) \end{array}\right] > 0 \tag{15}$$

3.2. Coiled Diameter Constraints from Volume Requirement

An important boom design consideration was the coiled diameter of the boom, which needed to satisfy a certain packaged volume requirement while stowed. The requirement translated to a maximum allowable outer diameter of the coil, D_f, which had to be satisfied by the Bi-CTM boom designs. The total thickness of all booms coiled, t_t, first had to be found through the following equation:

$$t_t = n_b t_m (1 + \mu), \tag{16}$$

where n_b was the total number of Bi-CTM booms coiled per spool, μ was the packaging efficiency parameter, and t_m was the largest inner and outer shell thickness between those of segments 1, 2, and the web section.

The total number of wraps in the coil, w_c, was found with (17), where the boom length L was already established and r_i was the initial coiled radius, assumed here to be the radius $1/C$ of the secondary stable state.

$$w_c = \sqrt{\left(\frac{r_i}{t_t}\right)^2 + \frac{L}{\pi t_t}} - \frac{r_i}{t_t}. \tag{17}$$

With w_c and t_t found, the outer diameter of the coil, D_f, of any boom design could be solved for in (18). The resulting outer diameter had to be less than or equal to the maximum allowable diameter for the boom to satisfy the volume requirement.

$$D_f = 2\,(r_i + w_c t_t) \tag{18}$$

3.3. Area Moments of Inertia and Torsional Constant

Besides evaluating the stability of Bi-CTM booms, determining their area moments of inertia about the principal axes I_{yy} and I_{zz} and torsional constant J was critical for fulfilling boom system requirements for bending and torsional stiffnesses. Optimal cross sectional geometries of the boom that maximized these metrics, and therefore the stiffnesses, were obtained through parametric analysis. The effective elastic and shear modulus of the boom was not considered since they only depended on the thin-ply material properties and laminates. In the extended configuration, the booms were oriented as shown in Fig. 1 (b). The origin of the $y - z$ coordinate system was placed at the geometric center of the cross section. Based on relevant geometric parameters such as the radii and lengths of circular arcs, flattened height, web length, and subtended angles, the boom's cross section was discretized into the (y, z) coordinates with simple trigonometry. Thus, each segment consisting of a pair of (y, z) coordinates was then idealized as a rectangle rotated an angle about the origin defined by β. The area moments of inertia of every segment about their own centroid relative to the y and z axes, I_{y_j} and I_{z_j}, were found with the following equations. Let any given rectangular segment be denoted with the subscript $j = 1, \dots, m$, where m was the total number of segments. l_j and t_j were the length and thickness of each segment.

$$I_{y_j} = \frac{1}{12} l_j t_j (l_j^2 \sin^2\beta + t_j^2 \cos^2\beta) \tag{19}$$

$$I_{z_j} = \frac{1}{12} l_j t_j (l_j^2 \cos^2\beta + t_j^2 \sin^2\beta) \tag{20}$$

The boom's area moments of inertia could be found by summing I_{y_j} or I_{z_j} through the parallel axis theorem, as shown in (21). A_j was the area of each segment and d_j was the distance from each segment's centroid to the y or z axis.

$$I_{yy,zz} = \sum_{j=1}^{m} I_{y,z_j} + A_j {d_j}^2 \tag{21}$$

The torsional constant was found by summing the torsional constants of the web as open sections J_O and the circular segments as the closed sections J_C as shown below. A_E was the total enclosed area in the closed section.

$$J_O = \sum_{j=1}^{m} \frac{1}{3} l_j {t_j}^3 \tag{22}$$

$$J_C = 4{A_E}^2 / \sum_{j=1}^{m} \frac{l_j}{t_j} \tag{23}$$

4. PARAMETRIC ANALYSES

With the analytical model derived for the Bi-CTM boom, a series of parametric studies were conducted to evaluate how geometric, material, and layup designs influence stiffness properties, bistability, and coiled diameters. Optimal cross-sections were obtained by maximizing the area moments of inertia and torsional constants while maintaining bistability and satisfying volume requirements. Specifically, the objective was to maximize I_{yy}, I_{zz}, and J while varying relevant design parameters such as the radii and subtended angle of various shell segments. Simultaneously, bistability was evaluated with the criterion in (13-15), and the outer coiled diameter constraint was evaluated with (18). The criterion value from (15) represented the concavity of the second strain energy well. A higher number meant that the boom would more easily reach and remain in the coiled configuration. Any data points which yielded a monostable boom or exceeded the volume requirement were removed from the analysis. Boom designs found to be favorable for both stiffness properties and bistability were fabricated and compared against model predictions for validation. Table 1 shows the material description and properties of the thin-ply composites and adhesive that were used for the parametric analysis and boom fabrication.

Table 1. Material properties of thin-ply composites and adhesive

Label	Material Description	Fiber/Resin	E_1 (GPa)	E_2 (GPa)	ν_{12}	G_{12} (GPa)	Lamina AW (g/m^2)	Thickness t (mm)
C	Unidirectional (UD) Carbon Fiber	MR60H / PMT-F7	174.40	8.39	0.259	6.40	63.4	0.040
PW_C	Plain Weave Carbon Fiber	M30S / PMT-F7	94.20	94.20	0.026	3.94	89.7	0.058
A	Hysol EA9628 Film Epoxy	N/A	2.14	2.14	0.712	0.62	146.0	0.100

Five boom cases differentiated by shell layup and geometry were evaluated in the parametric analysis and are summarized in Table 2. The boom cross-sections were symmetric as in Fig. 1 when the subtended angle and radii of both segments between the inner and outer shells were kept identical. However, asymmetric cross-sections where these parameters differ had the potential to yield booms with improved bistable characteristics. Placing bistable layups in segment 2 of the inner shell aided the bistable outer shell segment 1 in generating a second stable energy well, due to both segments bending in the equal-sense way relative to their extended configurations. This effect was amplified when the arc length and radius of segment 2 were dominant over segment 1 of the inner shell in asymmetric cross-sections. For every case, ply drops were incorporated between segments 1 and 2 in the outer shell to reduce the stiffness of the latter segment, which was monostable and helped negate the second strain energy well generated by segment 1. This was also implemented for the inner shell in case 5, where the ply drop in segment 1 aided segment 2 in yielding bistable configurations.

Table 2. Bi-CTM booms evaluated in parametric analysis.

Bi-CTM Case #	Outer Shell Segment 1	Outer Shell Segment 2 and Web	Inner Shell Segment 1	Inner Shell Segment 2 and Web	*h* (mm)	*w* (mm)
Symmetric						
1	[45PW_C/0C/45PW_C]	[0C/45PW_C]	[45PW_C/90C]	[45PW_C/45PW_C]	110	5
2	[45PW_C/0C/45PW_C]	[0C/45PW_C]	[45PW_C/90C]	[45PW_C/45PW_C]	130	4.5
3	[45PW_C/0C/45PW_C]	[0C/45PW_C]	[0-90PW]	[0-90PW]	110	5
Asymmetric						
4	[45PW_C/0C/45PW_C]	[0C/45PW_C]	[45PW_C/90C]	[45PW_C/45PW_C]	130	4.5
5	[45PW_C/0C/45PW_C]	[0C/45PW_C]	[45PW_C/0C]	[45PW_C/0C/45PW_C]	130	4.5

Each shell of the Bi-CTM boom had two independent geometric parameters that could be varied, the subtended angle of both circular segments and the radius of either segment. To prevent kinks between the arcs and maintain tangent continuity, the subtended angle of both segments had to be identical. If a radius was specified for one arc, then the other segment radius was set and could not be altered as determined by (1) and (2). For all parametric analysis, the subtended angle was varied from 50° to 90° with a 0.5° step size. Lower subtended angles more heavily favored I_{zz} over I_{yy} and J while lacking sufficient structural depth required for bistability. Cross-sections with higher subtended angles than 90° were difficult to manufacture and were not considered. For cases 1 and 3, the radius of segment 2 was varied from 8.67 mm to 48.6 mm in 1 mm intervals, where the lower value was a manufacturing and laminate strain to failure constraint and the upper limit was determined by the total arc length of segments 1 and 2 being 100 mm. This range corresponded to reducing the radius of segment 1 from 48.6 mm to 8.67 mm. For cases 2, 4 and 5 with a flattened height of 130 mm, the radius of segment 2 was varied from 12 mm to 57.3 mm, increasing the radius of segment 1 from 57.3 mm to 12 mm. The volume requirement dictated four co-wrapped CTM booms per spool, each with a length of 16.55 m, to not exceed an outer coiled diameter of 305 mm. A packaging efficiency of 60% was assumed.

4.1. Symmetric Cross-Sections

For symmetric cases, the variation of subtended angle and radii were identical between the inner and outer shells. Fig. 3 shows the area moments of inertia, torsional constant, bistability criterion values, and stable coiled diameters for the Bi-CTM case 1 against the variation of subtended angles and radii of the segments for both shells. Higher subtended angles favored I_{yy} and J while lower values were more suited for maximizing I_{zz} and the bistability criterion $\frac{\partial^2 \hat{U}}{\partial \theta^2}$. A larger segment 1 radius and the corresponding smaller segment 2 radius favored all metrics presented here. All boom configurations within the entire parameter range satisfied the coiled volume requirement. The lack of data points at very low segment 1 radius and high segment 2 radius at lower subtended angles indicated that these combinations of parameters yielded monostable booms. For cases 1 and 2 this was due to the inner shell segment 2 (bistable laminate [45PW$_C$/45PW$_C$]) not being able induce a second strain energy well due to being overcome by the outer shell segment 2's (monostable laminate [0$_C$/45PW$_C$]) stiffness when bent in the opposite-sense way. For large segment 1 radius values, this was irrelevant since the outer shell segment 1 was still able to generate bistability for the boom despite the inner shell segment 1 being monostable due to having lower strain energies. The Bi-CTM case 1 was the most bistable with a criterion value of 0.45 at the subtended angle of 50°, segment 1 radius of 48.6 mm, and segment 2 radius of 8.67 mm for both shells. These values yielded the largest ratio of arc lengths between segments 1 and 2, where longer segment 1 and shorter segment 2 lengths ensured higher criterion values since the former was bistable and latter was monostable for the outer shell. Since the extended boom had to be able to withstand loads in both the y and z directions during operation, the optimal cross-sectional geometry was that which yielded the maximum value for the area moment of inertia for the lower of the two directions, in this case I_{yy}. This ensured that the boom would retain adequate bending stiffness regardless of the load direction. For the Bi-CTM case 1, I_{yy} was maximized when the subtended angle is 90°, radius of segment 1 was 23.16 mm, and the radius of segment 2 was 8.67 mm for both shells. This led to 10,807 mm^4 for I_{yy}, 12,597 mm^4 for I_{zz}, 15,376 mm^4 for J, a 75.87 mm inner coiled diameter, and a bistability criterion value of 0.37. Although this boom conflicted with the design yielding the highest bistability criterion value, it still retained a favorable criterion value compared to the corresponding maximum. For this optimal geometry, the polar contour plot of the non-dimensional bending strain energy per unit length, $\hat{U}$, is presented in Fig. 4 (a). The two equilibrium locations are marked as black dots. The first one, which had zero strain energy, corresponding to the as-manufactured relaxed and extended state, was always located at $\theta = 0$ and $\hat{C} = 1$. The second strain energy well, corresponding to the stable coiled configuration, was located at $\theta = \frac{\pi}{2}$ and a certain radius, r_i, defined by $\hat{C} = CR_{1_O}$, where $r_i = 1/C$.

Figure 5 shows the area moments of inertia, torsional constant, bistability criterion values, and stable coiled diameters for the Bi-CTM case 2 against the variation of subtended angles and radii of the segments for both shells. With the only differences between cases 1 and 2 being the flattened height, web width, and the range of radii values, the moments of inertia, torsional constant, and bistability criterion results for case 2 showed the same trends as case 1. Again, all boom configurations satisfied the volume constraint. Since case 2 had a larger cross-section geometry, the resulting I_{yy}, I_{zz}, and J values were larger while the bistability criterion values were identical due to its dependence on the shell bending stiffnesses and normalized radii and arc lengths. The optimal configuration, where I_{yy} was maximized, was when the subtended angle was 90°, radius of segment 1 was 26.5 mm, and the radius of segment 2 was 12 mm for both shells. This led to 18,710 mm^4 for I_{yy}, 19,771 mm^4 for I_{zz}, 25,287 mm^4 for J, a 86.1 mm coiled diameter, and criterion value of 0.37.

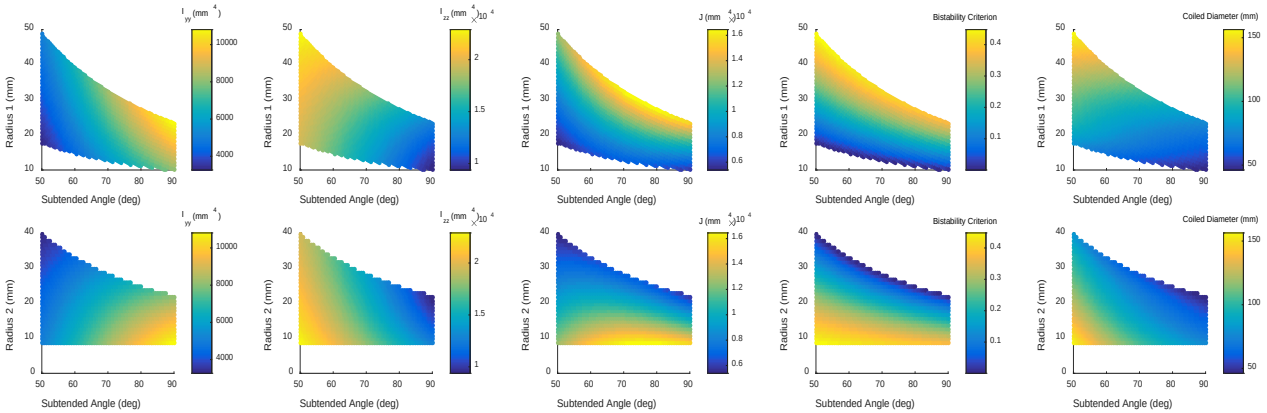

Fig. 3. Symmetric Bi-CTM case 1 parametric analysis with I_{yy}, I_{zz}, J, and bistability criterion $\frac{\partial^2 \hat{U}}{\partial \theta^2}$ as metrics and α, R_1, and R_2 as input parameters.

As with the Bi-CTM case 1, the optimal geometry for case 3, where I_{yy} was maximized, was when the subtended angle was 90°, radius of segment 1 was 23.16 mm, and the radius of segment 2 was 8.67 mm for both shells. This led to 8,087 mm^4 for I_{yy}, 10,037 mm^4 for I_{zz}, 10,739 mm^4 for J, a 66.97 mm inner coiled diameter, and a criterion value of 0.63. The stiffness values were lower than case 1 due to the thinner inner shell laminate. For this optimal geometry and case 3 laminate configuration, the polar contour plot of the non-dimensional bending strain energy per unit length, $\hat{U}$, was presented in Fig. 4 (b). Note that the second strain energy well of the coiled state of case 3 was deeper than in case 1, as represented by the contour lines separated by a constant $\widehat{\Delta U} = 0.05$ in Fig. 4, even though the geometries were the same. This was in line with the larger bistability criterion value for case 3 of 0.63 compared to case 1 (and 2) of 0.37. Both case 1 and 3 shared the same optimal geometry and outer shell laminate construction. Thus, the less stiff inner shell of case 3 (monostable laminate [0-90PW$_C$]) compared to case 1 resulted in a more compliant boom half that disrupted less the bistable outer shell when coiled.

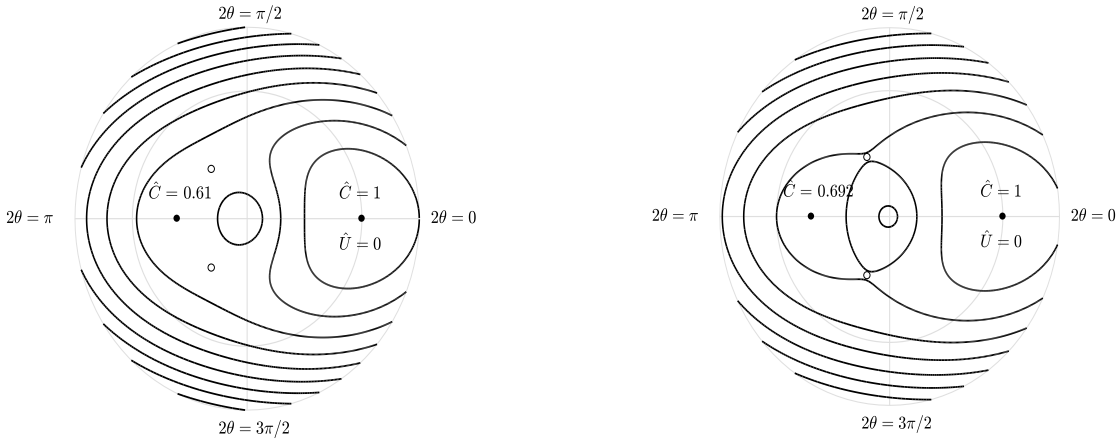

Fig. 4. Polar contour plot of the non-dimensional bending strain energy per unit length, $\hat{U}$, as a function of the non-dimensional coiled curvature, $\hat{C}$, and the angle of the shell relative to an underlying cylinder, θ, for (a) the Bi-CTM case 1 optimal geometry, and (b) the Bi-CTM case 3 optimal geometry. The two stable equilibrium locations are marked as dots while the two unstable points are marked as circles. The contour lines are separated by a constant $\widehat{\Delta U} = 0.05$.

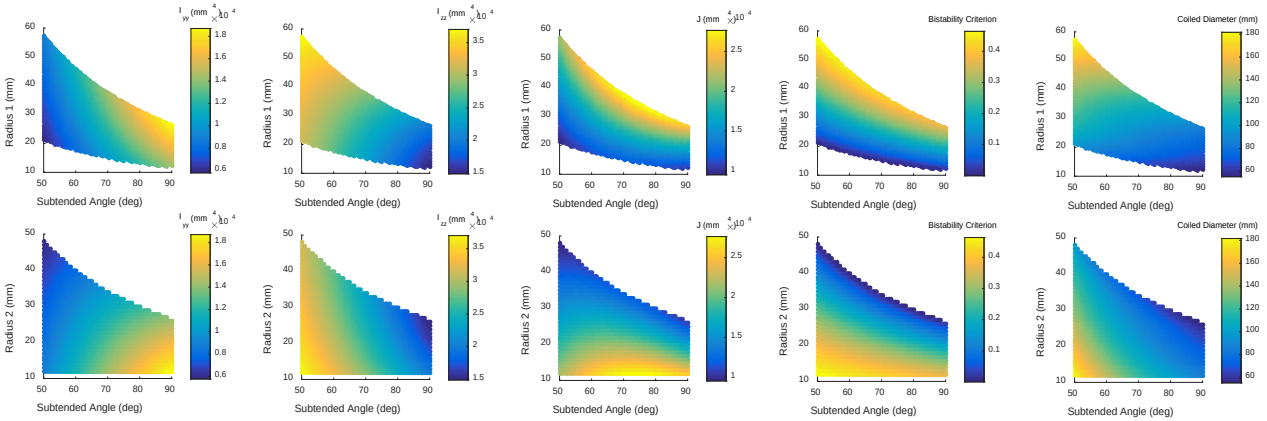

Fig. 5. Symmetric Bi-CTM case 2 parametric analysis with I_{yy}, I_{zz}, J, and bistability criterion $\frac{\partial^2 \hat{U}}{\partial \theta^2}$ as metrics and α, R_1, and R_2 as input parameters.

4.2. Asymmetric Cross-Sections

The motivation for asymmetric cases was to yield booms with higher bistability criterion values at the expense of stiffness properties. The outer shell geometry remained fixed at a subtended angle of 90°, segment 1 radius of 26.5 mm, and segment 2 radius of 12 mm, which corresponded to the optimal configuration yielding the maximum I_{yy} as seen for the symmetric case 2 of equal flattened height of 130 mm. Fig. 6 shows the area moments of inertia, torsional constant, bistability criterion values, and stable coiled diameters for the Bi-CTM case 4 against the variation of subtended angles and radii of the segments for the inner shell.

Similar to cases 1 through 3, larger subtended angles favored I_{yy} and J while smaller values were more suited for maximizing I_{zz} for the inner shell. In addition, their maximum values were only slightly lower than case 2, which had identical shell layups as case 4 but with a symmetric cross-section. The boom geometry where I_{yy} was maximized was identical to that of case 2 due to sharing the same parameters for this particular configuration. More interestingly, the large differences could be seen in the bistability criterion values and the range of bistable data points. The criterion values were higher over the parameter range due to the arc length and radius of the bistable inner shell segment 2 being increased while those of the monostable inner shell segment 1 being decreased, and simultaneously the bistable outer shell segment 1 length remained maximized at the subtended angle of 90°. This manipulation of arc lengths allowed the bistable segments bending in the equal-sense way to be fully dominant over their less stiff monostable counterparts bending in the opposite-sense way. The CTM booms became monostable if the inner shell segment 2 radius was low and the segment 1 radius was high at lower subtended angles, due to the difference of arc lengths between the two exceeding that of the outer shell. The maximum criterion value was 3.64 at a subtended angle of 50°, segment 1 radius of 12 mm, and segment 2 radius of 57.3 mm for the inner shell. This configuration yielded the largest difference between the arc lengths of segment 2 and segment 1 for the inner shell, where the former was larger than the latter. In the interest of retaining favorable stiffness and bistable properties with the asymmetric design, the optimal configuration was chosen to be at a subtended angle of 90°, segment 1 radius of 12 mm, and segment 2 radius of 26.5 mm for the inner shell. This yielded 16,760 mm^4 for I_{yy}, 18,137 mm^4 for I_{zz}, 17,963 mm^4 for J, a 70.46 mm inner stable coiled diameter, and a criterion value of 1.29. The larger criterion value over case 2 (0.37) demonstrated that the asymmetric cross-sections were better candidates for generating bistability.

Fig. 7 shows the area moments of inertia, torsional constant, bistability criterion values, and stable coiled diameters for the Bi-CTM case 5 against the variation of subtended angles and radii of the segments for the inner shell. Compared to case 4, the area moments of inertia and torsional constants exhibited the same trends and were greater in magnitude due to the thicker inner shell laminate. In addition, the bistability trends were identical, but the criterion values were greater due to the bistable inner shell segment 2 layup, which matched that of the outer shell segment 1, being more bistable and stiffer than that from case 3. This meant that when both segments are bent in the equal-sense way, their resulting second strain energy well locations are closer to each other compared to the Bi-CTM case 3. The optimal geometry which yielded favorable stiffness and bistable properties was identical to that of case 4. This yielded 17524 mm^4 for I_{yy}, 19758 mm^4 for I_{zz}, 19610 mm^4 for J, a 69.73 mm inner stable coiled diameter, and a bistability criterion value of 1.83.

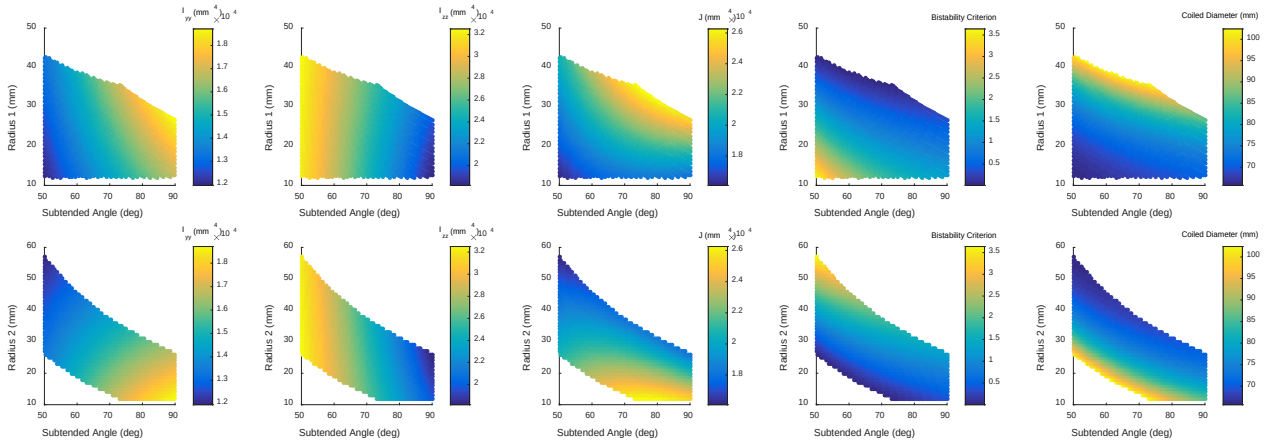

Fig. 6. Asymmetric Bi-CTM case 4 parametric analysis with I_{yy}, I_{zz}, J, and bistability criterion $\frac{\partial^2 \tilde{U}}{\partial \theta^2}$ as metrics and α, R_1, and R_2 as input parameters.

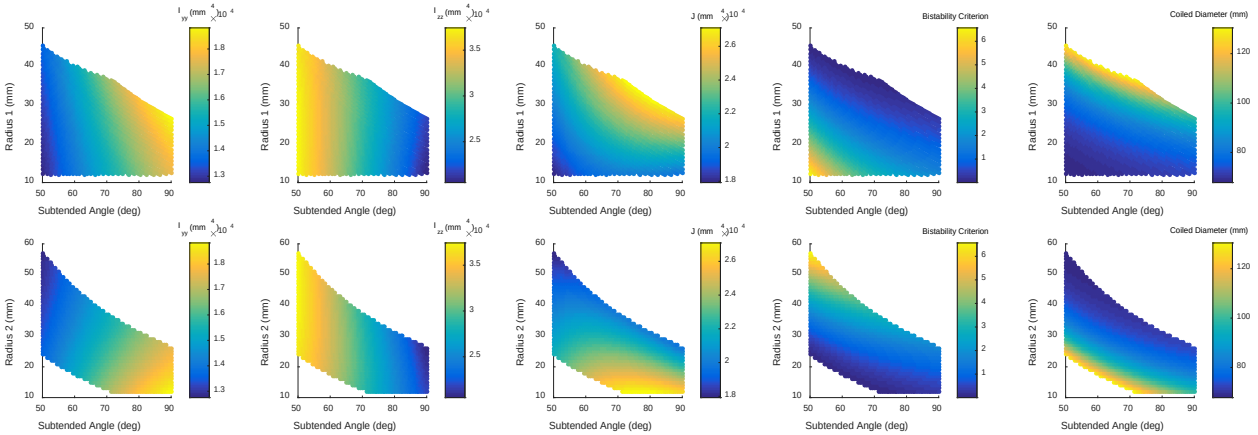

Fig. 7. Asymmetric Bi-CTM case 5 parametric analysis with I_{yy}, I_{zz}, J, and bistability criterion $\frac{\partial^2 \tilde{U}}{\partial \theta^2}$ as metrics and α, R_1, and R_2 as input parameters.

5. MODEL AND TEST RESULTS COMPARISON

Boom specimens with the optimal geometries and shell laminates of Bi-CTM cases 1, 3, 4 and 5 were manufactured to evaluate the bistability analytical model developed by comparing the predicted and measured stable coiled diameters, as well as assess if the model was able to correctly distinguish between bistable and monostable configurations. Bi-CTM cases 1 and 2 are essentially identical other than the larger geometry of case 2 represented by the bigger flattened height of 130 mm versus the 110 mm of case 1, and thus case 2 was not fabricated. The molds used to fabricate boom specimens for the Bi-CTM symmetric cases 1 and 3 had a subtended angle of $\alpha = 85°$, whereas those for asymmetric cases 4 and 5 had a subtended angle of $\alpha = 90°$. Thus, the symmetric cases differed slightly from the optimal designs with an angle of $\alpha = 90°$ analysed in Section 4.1.

Several parameters affected the as-manufactured booms in terms of matching intended optimal shapes, the most critical one being the thinness of the laminates involved and the relatively large radii involved that did not provide much structural depth to the parts. Using asymmetric laminates for some of the shell segments also translated to thermo-elastic deformations during the boom curing process at high temperatures that resulted in permanent deformations once the parts returned to room temperature. The coefficient of thermal expansion (CTE) mismatch between the part and the mold also produced a similar effect on the final shape of the boom structure. Both of these effects were exacerbated by the small wall thickness of the shells. Finally, the asymmetric nature of the boom laminate design tended to result in the stiffer half slightly bending the softer half at the bonded web, which deformed the cross-section and introduced asymmetry, even for the symmetric cases. Therefore, in an effort to be consistent between what was being modelled and the test article, the as-manufactured geometry of the booms was measured by image processing. Photographs of the cross-section of both boom ends were taken and tangent circles were fitted to the geometry to determine the average radius of each shell segment for both the inner and outer walls as shown in Fig. 8. With the measured radii, the subtended angle for each shell was calculated using (2). The web width and flattened height remained unchanged during fabrication and were identical to the desired ones listed in Table 2.

Table 3 shows the averaged geometric parameters measured for all Bi-CTM boom specimens manufactured. In addition, the bistability criterion values for the imperfect geometries are shown as well as the predicted coiled diameters and the measured ones. The differences between the theoretical and empirical values for the boom's stable coiled diameter are also presented. It can be seen that for all cases studied the inner shell segments had larger subtended angles than the outer shell segments. This represented a departure from symmetry where the straight web segments were not parallel after manufacturing due to the thinner and less stiff inner shells collapsing slightly towards the boom cavity, and evident in Fig. 8 (b) and (c) as the outer shell flattens while the inner shell bulges. As expected, the asymmetric boom cases were more bistable than the symmetric ones. The bistability criterion values, S, of the symmetric cases with imperfect geometries were larger than the ideal ones for $\alpha = 85°$ because of the increase in outer segment 1 radius with respect to the ideal case, particularly for case 3. The criterion values of the asymmetric cases with imperfect geometries were smaller than the ideal ones for $\alpha = 90°$ because the arc lengths corresponding to the bistable segments coiling in an equal sense-way (outer segment 1 and inner segment 2) had decreased slightly, particularly for case 5, although case 5 still showed the largest criterion value of all cases. The differences between the predicted and the measured values of the second stable coiled diameter for all cases evaluated were between 26.9% and 33.1%, with the analytical model under-predicting them.

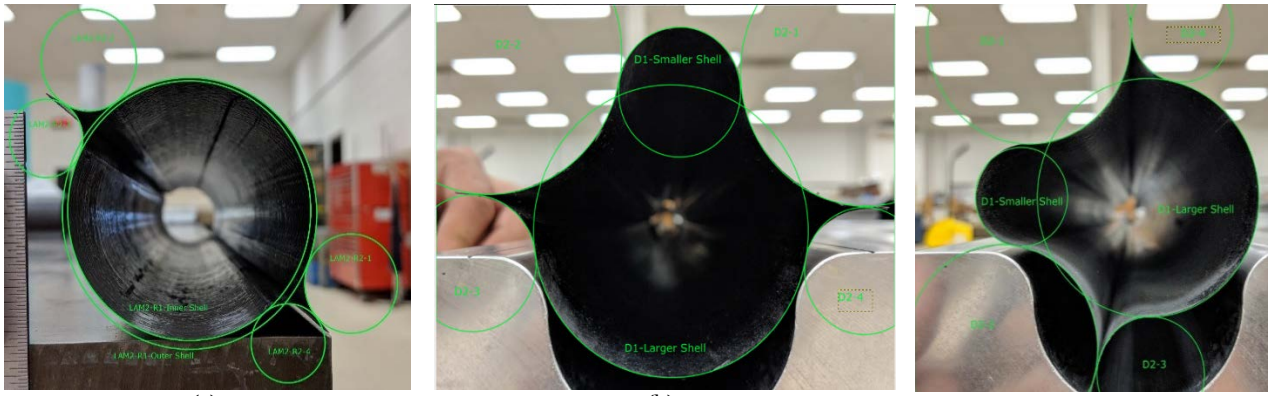

(a) (b) (c)

Fig. 8. As-manufactured cross-section of various bi-CTM booms with the fitted tangent circles for each shell segment in green for: (a) case 1; (b) case 4; and (c) case 5.

Table 3. Geometry of the as-manufactured Bi-CTM booms and shells evaluated, model predictions and measured values.

Bi-CTM Case #	Avg. Outer Segment 1 Radius, R_{1_O} (mm)	Avg. Outer Segment 2 Radius, R_{2_O} (mm)	Outer Subt. Angle, α_O (°)	Avg. Inner Segment 1 Radius, R_{1_I} (mm)	Avg. Inner Segment 2 Radius, R_{2_I} (mm)	Inner Subt. Angle, α_I (°)	Bistability Criterion Value, S	Predicted Coiled Diameter, $D_{i,theo}$(mm)	Measured Coiled Diameter, $D_{i,exp}$(mm)	Error Coiled Diam., ε_D (%)
Symmetric										
1	26.79	9.90	79.67	25.59	7.75	87.65	0.40	85.94	117.58	26.91
3	30.25	10.67	71.40	28.59	9.30	77.14	0.70	85.68	128.12	33.13
Asymmetric										
4	28.59	13.23	82.88	12.88	26.70	87.57	1.21	76.53	112.88	32.20
4 Outer Shell	28.59	13.23	82.88	-	-	-	0.91	75.27	89.48	15.88
4 Inner Shell	-	-	-	12.88	26.70	87.57	0.31	78.71	91.74	14.20
5	28.14	13.32	83.61	12.02	24.62	94.59	1.54	74.70	102.42	27.07
5 Outer Shell	28.14	13.32	83.61	-	-	-	0.89	74.26	80.69	7.97
5 Inner Shell	-	-	-	12.02	24.62	94.59	0.66	74.55	76.54	2.60

Fig. 9 shows the polar contour plot of the non-dimensional strain energy per unit length for the Bi-CTM case 4 and its outer and inner shells coiled alone. After measuring the Bi-CTM case 4 coiled diameter, the boom was split apart into its two constituent shells, which were then coiled individually. While the analytical model under-predicted by 32.2% the coiled diameter corresponding to the location of the second strain energy well for case 4 with both bonded shells co-wrapped, the disparity reduced to 15.8% and 14.2% for the case 4 outer and inner shells coiled alone.

Fig. 10 shows the strain energy polar contour plot for the Bi-CTM case 5 and its outer and inner shells coiled individually. While the analytical model under-predicted by 27.1% the coiled diameter of the second strain energy well for case 5 with both bonded shells co-wrapped, the disparity decreased to 8.0% and 2.6% for the case 5 outer and inner shells coiled alone. The much lower error values of the individually coiled boom halves meant that the simple inextensional bending model developed was more accurate when the deformations were analysed for single-shell structures. There were three main reasons for this. First, the simple model did not account for the extra strain energy generated by connecting or bonding shell segments with different individual strain energies in the coiled configuration. The bistability criterion values of the complete CTM boom were simply the sum of the criterion values for the two individual shells. Second, the friction between both boom walls was not modelled. Third, in the specimens fabricated, wrinkling or local buckling of the inner shell when the boom was coiled was observed, and the additional strain energy for that discrete local deformation was not included in the model. Thus, for better predictions of the Bi-CTM boom's coiled diameter, the model would need to be extended to include those additional deformations and forces that contributed to the total strain energy of the system. The prediction errors for the individual shells could be attributed mainly to some geometric difference between the model and the specimens, as well as errors in the constituent properties of the thin-ply composite materials assumed in the model.

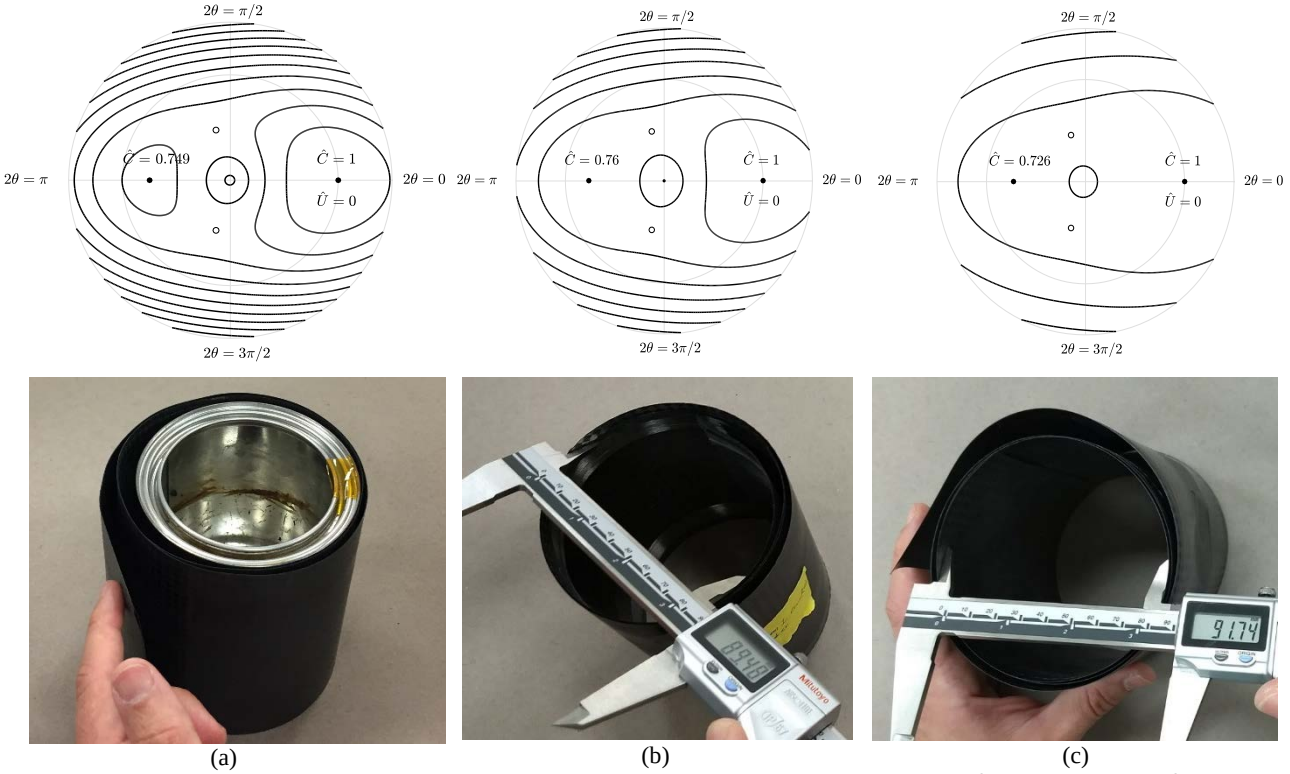

Fig. 9. (Top) Polar contour plot of the non-dimensional bending strain energy per unit length, $\widehat{U}$, as a function of $\widehat{C}$ and θ for the as-manufactured geometry of (a) Bi-CTM asymmetric case 4, (b) case 4 outer shell individually, and (c) case 4 inner shell individually. The two stable equilibrium locations are marked as dots while the two unstable points are marked as circles. The contour lines are separated by a constant $\Delta\widehat{U} = 0.05$. (Bottom) Aforementioned case 4 shells specimens in the coiled state.

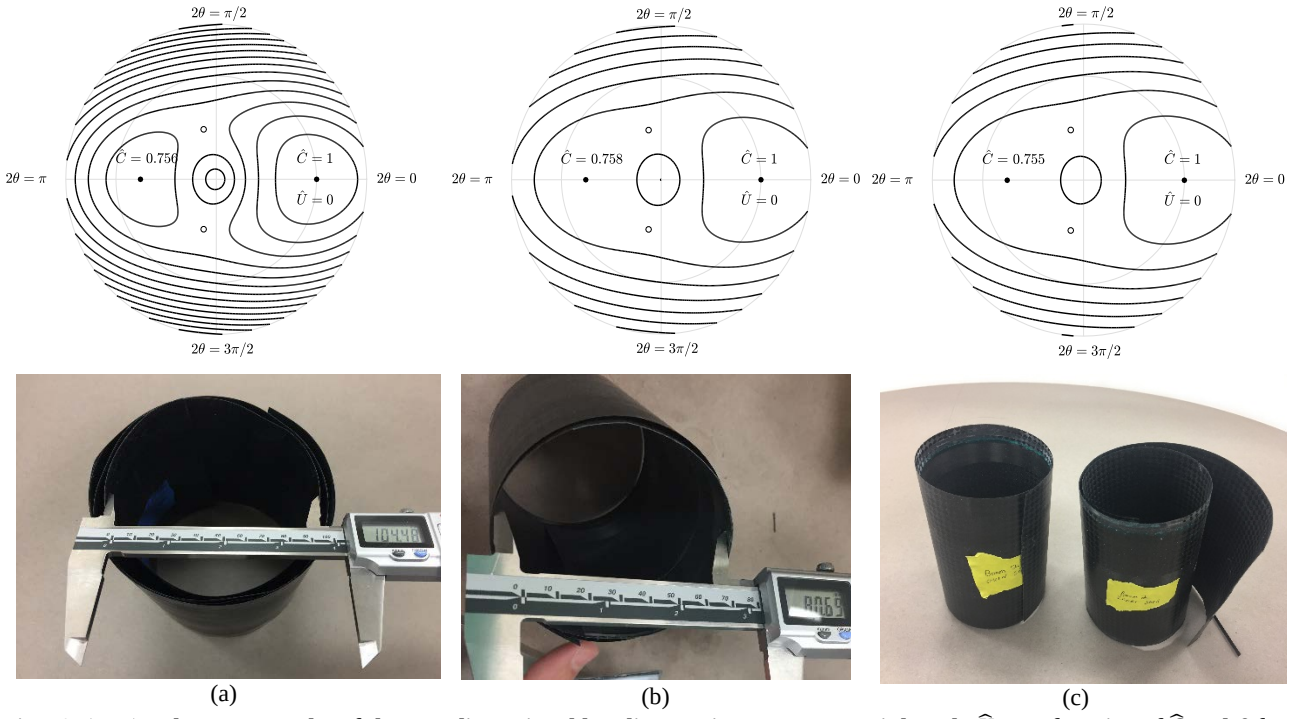

Fig. 10. (Top) Polar contour plot of the non-dimensional bending strain energy per unit length, $\widehat{U}$, as a function of $\widehat{C}$ and θ for the as-manufactured geometry of (a) Bi-CTM asymmetric case 5, (b) case 5 outer shell individually, and (c) case 5 inner shell individually. The two stable equilibrium locations are marked as dots while the two unstable points are marked as circles. The contour lines are separated by a constant $\Delta\widehat{U} = 0.05$. (Bottom) Aforementioned case 5 shells in the coiled state. (c) Case 5 outer and inner shells side by side.

For all cases studied, the outer shell contributed more to the bistability of the entire boom, as was represented by a larger criterion S value compared to the inner shell one. Given the identical but reversed laminate construction between segments 1 and 2 for the inner and outer shells of Bi-CTM case 5, the predicted coiled diameters of the individual shells and the complete boom were practically the same. This can be seen in Fig. 10 (b) and (c) where the strain energy contour plots of the individual shells were close. Also in Fig. 10 (c) bottom picture, where both the case 5 outer and inner coiled shells rested side by side. The Bi-CTM case 4 showed a larger difference between the coiled diameters of the individual shells and that of the complete boom as each shell's laminate was different. Fig. 9 (b) and (c) presented different strain energy fields for the outer and inner shells of case 4 with a different $\hat{C}$ value at location of the second energy well. The complete boom's stable coiled diameter value was between that of its individual shells wrapped alone.

6. CONCLUSIONS

This research and development effort was intended to initially generate bistable configurations for the structural efficient, closed-section, two-shelled CTM rollable boom. The boom concept is a promising candidate for NASA for various deployable structural systems to be compactly stored on small satellite platforms for a wide range of applications and missions. Bistable rollable booms are stowed in a lower energy stable state than its monostable counterparts and the release of strain energy during extension to the zero energy, stress-free boom configuration is more controlled and reliable, which enables more compact and lighter self-deployment structural concepts.

A simple inextensional analytical model describing the bending deformation mechanics of CTM booms was developed to determine how design variables induce bistability, or the existence of two strain energy wells. In this two-parameter model, the bending strain energy of the different circular and flat shell segments that form the boom cross-section are calculated separately and then combined in the energy minimization formulations. A bistability criterion was derived to evaluate bistability of the second equilibrium coiled state in order to determine which design parameters were critical for inducing bistability. The diameter of the coiled state and the bistability criterion depended on the arc lengths and radii of every circular segment, the web length, and the bending stiffnesses of both shells. The criterion allowed the direct evaluation of bistability without the need for minimizing the strain energy, which was particularly useful during parametric studies where the complete boom design space was explored.

For several laminate designs that were previously prone to induce bistability in similar two-shelled boom structures (12), the full design space of symmetric and asymmetric CTM boom cross-sections was parametrically analyzed. Higher subtended angles of the circular shell segments favored I_{yy} and J, while lower values were more suited for maximizing I_{zz} and the bistability criterion. For the symmetric cases, a larger segment 1 radius with the bistable laminate and the corresponding smaller segment 2 radius favored all metrics presented including bistability. The structurally optimal symmetric case with the thinnest and less stiff inner shell had the deepest second energy well, though at the expense of overall boom stiffness. A more compliant monostable inner-half favored bistability. Designing the boom cross-section asymmetrically was found to be a good way to favor bistability, as these cases generally had larger criterion values than the symmetric cases, though at the expense of overall boom stiffness. However, the structurally optimal asymmetric cases evaluated, which had a subtended angle of 90°, did not have much lower stiffnesses than the symmetric ones with identical shell layups, but had significantly larger bistability criterion values. The manipulation of arc lengths in the asymmetric cases allowed the bistable segments bending in the equal-sense way to be longer and fully dominant over their shorter and less stiff monostable counterparts bending in the opposite-sense way.

Several optimized Bi-CTM boom designs were fabricated and used to evaluate the validity of the analytical model developed. The booms modeled included the imperfections measured in the as-manufactured booms, result of the fabrication process that induced deformations on the thin-shells. For all cases, the inner shell segments had larger subtended angles than the outer shell segments. As predicted by the model, the asymmetric boom specimens fabricated were more bistable than the symmetric ones, being more prone to remain coiled without applying any radial constraints. The differences between the predicted and the measured values of the second stable coiled diameter for all Bi-CTM boom cases evaluated were between 27% and 33%, with the analytical model under-predicting the coiled diameter. However, the disparity reduced significantly when coiling alone one half of the boom. The differences were as low as 8% and 2.6% for one of the cases' outer and inner shells coiled individually. For better predictions of the Bi-CTM boom's coiled diameter and strain energy field, the simple model would need to be extended to include additional observed local deformations like wrinkling or local buckling of the inner shell, as well as friction between both boom walls and different segment-to-segment connecting/bonding forces that contribute to the total strain energy of the system. The constituent properties of the thin-ply composite materials and adhesive bond layer assumed in the model might also have been an additional source of error.

ACKNOWLEDGEMENTS

This research was sponsored by NASA's Space Technology Mission Directorate (STMD) under a Game Changing Development Program (GCDP) project to advance deployable thin-shell composite boom technology [8]. Andrew J. Lee was supported by the NASA Internships, Fellowships, and Scholarships (NIFS) Program at NASA LaRC. Help with boom specimen manufacturing from the Advanced Composites Fabrication Lab technicians at NASA LaRC, Kevin J. McLain and Mark Griffith, is gratefully acknowledged.

REFERENCES

[1]. B.B. Rennie, "New Closed Tubular Extendible Boom", *2nd Aerospace Mechanisms Symposium,* ed: Herzl, G.G., JPL TM 33-355, pp.163-170, 1967.

[2]. D.S. Crouch, "Mars Viking Surface Sampler Subsystem", *25th Conference on Remote Systems Technology*, 1977.

[3]. H.H. Armstrong, R.R. Johnson, "Organic & Metal Matrix Composites for Spacecraft Applications", *SAMPE Quarterly*, 1978.

[4]. M.A. Aguirre-Martinez, R. Bureo-Dacal, F. Del Campo, M. Fuentes, "The CTM family of Masts and the CTM Engineering Model", *3rd European Space Mechanisms & Tribology Symposium*, Madrid, Spain, 1987.

[5]. M.A. Aguirre-Martinez, D.H. Bowen, R. Davidson, R.J. Lee, T. Thorpe, "The Development of a Continuous Manufacturing Method for a Deployable Satellite Mast in CFRP", *British Plastics Congress*, pp. 107-110, 1986.

[6]. U. Geppert, B. Biering, F. Lura, J. Block, M. Straubel, R. Reinhard, "The 3-step DLR-ESA Gossamer Road to Solar Sailing", *Advances in Space Research*, Vol. 48, pp. 1695-1701, 2011.

[7]. M. Hillebrandt, C. Huhne, "The Boom Design of the De-Orbit Sail Satellite", *13th European Conference on Spacecraft Structures, Materials and Environmental Testing*, Braunschweig, Germany, 2014 (ESA SP-727, June 2014).

[8]. NASA Space Technology Mission Directorate, Game Changing Development Program, URL: http://gameon.nasa.gov/projects/deployable-composite-booms-dcb

[9]. J.M. Fernandez, "Advanced Deployable Shell-Based Composite Booms for Small Satellite Applications including Solar Sails", *4th International Symposium on Solar Sailing*, Kyoto, Japan, 17-20 Jan. 2017.

[10]. J.M. Fernandez, et al., "An Advanced Composites-Based Solar Sail System for Interplanetary Small Satellite Missions", *5th AIAA Spacecraft Structures Conference, AIAA Scitech 2018 Forum*, Kissimmee, FL, 8-12 Jan. 2018.

[11]. J.M. Fernandez, et al., "NASA's Advanced Solar Sail Propulsion System for Low-Cost Deep Space Exploration and Science Missions that Use High Performance Rollable Composite Booms", *4th International Symposium on Solar Sailing*, Kyoto, Japan, 17-20 Jan. 2017.

[12]. A.J. Lee, J.M. Fernandez, "Mechanics of Bistable Two-Shelled Composite Booms", *5th AIAA Spacecraft Structures Conference, AIAA Scitech 2018 Forum*, Kissimmee, FL, 8-12 Jan. 2018.

[13]. S.D. Guest, S. Pellegrino, "Analytical Models for Bistable Cylindrical Shells". *Proceedings of the Royal Society A*, Vol. 462, 2006, pp. 839-854.